ClinicSearch

Clinical Reviews and Case Reports

Delia Teresa Sponza *

Open Access

Research Article

Treatment Of Polyvınyl Chloride (Pvc), Polypropylene (Pp) Mıcroplastics, Usıng Bi2wo6 / Fe_3O_4 Nanocomposıte

Delia Teresa Sponza

Dokuz EYLÜL University, Engineering Faculty, Environmental Engineering Department, Buca İzmir Turkey.

***Correspondence Author:** Delia Teresa Sponza, Dokuz EYLÜL University, Engineering Faculty, Environmental Engineering Department, Buca İzmir Turkey.

Received Date: June 25, 2024 | Accepted Date: July 18, 2024 | Published Date: August 05, 2024

Citation: Delia T. Sponza, (2024), Treatment Of Polyvınyl Chloride (Pvc), Polypropylene (Pp) Mıcroplastics, Usıng Bi2wo6 / Fe_3O_4 Nano composıte, *Clinical Reviews and Case Reports*, *3*(4); **DOI:**10.31579/2835-7957/089

Abstract

Microplastics are ubiquitous in our daily life because of their low cost, portability, durability, and processability. However, since their chemical inert character and their accumulation problems exhibited a great threat to the sustainable development and ecocystem. Photo degradation of microplastic is a clean removal green technology. Therefore, in this study polyvinyl chloride (PVC), polypropylene (PP) microplastics was photodegraded with a novel heterogenous nanocomposite namely Bi_2WO_6 / Fe_3O_4 nanocomposite. The effects of increasing Bi_2WO_6 / Fe_3O_4 nanocomposite concentrations, PP and PVC concentrations, photodegradation time, pH, temperature on the photodegradation yields of PP and PVC yields were examined.For maximum PVC and PP yields (99% and 98%) the optimized conditions were as follows: Ph=5, 1.5 mg/l Bi_2WO_6 / Fe_3O_4 nanocomposite concentration, 800 mg/l PVC and PP concentrations, 15 min photodegradation time, 40 W/m2 sun ligth power, 30 Oc temperature and 0,9 mg/l Cl-1, SO4-2, BrO3-1, PO4-3 and CO3-2 ion concentrations. The XRD analysis showed that the cristal structure of **Fe_3O_4/Bi_2WO_6 nanocomposite** originated from the Bi_2WO_6 not from Fe_3O_4. The XPS disturbances of **Fe_3O_4/Bi_2WO_6 nanocomposite** showed the presence of Fe, W, O, and Bi elements.TEM and SEM imaged showed that the **Fe_3O_4/Bi_2WO_6 nanocomposite** exhibited a palm shape with **uniform structure of Bi and Fe.** HR-TEM analyses showed that the nanocomposite exhibited a 2D (dimensional)-2D heterostructure..

Keywords: bi_2wo_6 / fe_3o_4; nanocomposite; olyvinyl chloride (pvc); polypropylene (pp); photooxidation; microplastic

Introduction

Polyvinyl chloride (PVC) and polypropylene (PP), as engineering plastics, are extensively used in life and industry .They are found as microplastic in aquatic, marine, and soil environments. PVC and related plastic products are non-biodegradable in natural environment because of their chemical inertness(1). The PVC plastics become one of the main sources of “white pollution”. Traditional processing methods, such as garbage deposit or incineration, cause a serious secondary pollution. Therefore, the development of degradable PVC plastics becomes an important issue. There are some disadvantages in these PVC plastics, mainly the long degradation cycle and the incompleteness of the degradation, which limit their practical applications(2). Polyvinyl Chloride (PVC or Vinyl) is an economical and versatile thermoplastic polymer. It is widely used in the building and construction industry to produce door and window profiles. It also finds use in:drinking and wastewater pipes, wire and cable insulation, medical devices, etc. It is the world’s third-largest thermoplastic by volume after polyethylene and polypropylene(3-6). It is a white, brittle solid material available in powder form or granules. PVC is now replacing traditional building materials in several applications. These materials include wood, metal, concrete, rubber, ceramics, etc. in several applications. This is due to its versatile properties such as: lightweight, durable, low cost, and easy processability. Polypropylene (PP) is a type of polyolefin that is slightly harder than polyethylene. It is a commodity plastic with low density and high heat resistance. It finds application in packaging, automotive, consumer goods, medical, cast films, etc(7-9). A lot of studies showed that MP pollution in the surface water consisted of polypropylene (PP), and polyvinyl chloride (PVC). The pollution of these MPs cause to diferent interactions affecting their migration and transformations(10-12). The photodegradation of MPs in the environment during solar irradiation and the photolyzis of PP and PVC and OH radical production via ultraviolet ligth is an phenomenon. As a result, that the photolyzis PP and PVC were feasible process during their photodegradation. The photodegradable PVC and PP by some photocomposites exhibited their ability to decomposibiliy properties It is important to note that the during the photocatalytic degradation of PVC And PP dioxins were not produced and the decomposition intermediates were not toxic to the environmental ecocystems(13-20). It has been reported that reactive oxygen species produced from the photodegradation of irradiated PP and PVC MPs increases the absorption of UV energy(21-25. During irradiation of MP the release of volatile and dissolved organic

matters can be performed. Although $Fe_3O_4/SiO_2/TiO_2$ nanocomposites with enhanced photocatalytic activity and fast magnetic separability can be used in the photodegradation of PP and PVC low removal yields was detected. Fe_3O_4/metal hybrid nanostructures with polymers as such as Fe_3O_4@C@Cu_2O nanostructure can be used in the microplastics degradation. However, the synthesis of these magnetic nanocomposites requires some linker organics like silica, polymers, carbon making the synthesis more favorable and decrease the saturation magnetization (M_s) of the generated nanocomposites. Some magnetic nanocomposites like Fe_3O_4@Bi_2O_3 and Fe_3O_4/WO_3 can be used in the photodegradation of some organics(26-30). Fe_3O_4 exhibited rapid recombination of photogenerated carriers. The Z-scheme heterojunction exhibited ultimate light absorption capacity and goog separation yield of charge carriers has magnetic properties and can cause easy to recover the nanocomposite. The Fe_3O_4 can adhere to the semiconductor material and Fe_3O_4 can directly contact with Bi_2WO_6 to form heterojunctions. This increase the photodegradation yields by elevated increases the contact area between the two substances ending with high electron transfer to the pollutants(18-22) . Bi_2WO_6 has a hydrophilic surface, can be dispersed in water is simple, cheap and high stable. Previous studies have already demonstrated that Bi_6WO_{12} exhibited higher optical absorption at a wavelength above 440 nm than Bi_2O_3 or WO_3, by enhancing the photocatalytic activity under solar illumination . The structure of Bi_2WO_6 exhibited crystalline properties and is generated by $(Bi_2O_2)_n^{2n+}$ layers and perovskite-like $(WO_4)_n^{2n-}$ layers. However, However some times exhibited low photocatalytic activity in visible light region and the separation and recovery of this nano metal oxide was not possible(32-34). Magnetic separation provides an effective way for recycling the magnetic composites by providing appropriate external magnet areas. Supermagnetic Fe3O4 was associated with the photocatalyst to obtain a recoverable composite. The magnetic Fe3O4-Bi2WO6 was used in β-cyclodextrin (β-CD) removal with high-efficiency as carrier separation and semiconductor stabilization(35-38). The photodegradation yields of pollutants can be attributed to the its hydrophilic external surface, hydrophobic interior, and specific cavity diameter. Fe3O4-Bi2WO6 nanocomposite was used in the photocatalytic degradation of sunset yellow dye, of sulfamethoxazole, phenol, and rhodamine B dyes. However Fe3O4-Bi2WO6 nanocomposite was not used yet for the photodegradation of micropollutants(39-40). Therefore, in this study it was aimed to detect the photocatalytic capacities of PVC and PP microplastics under sunligth by using Fe3O4-Bi2WO6 nanocomposite. The photodegradation yields were investigated and the impacts of different reaction factors on the photodegradation, such as the amount of photocatalyst, the initial concentration of PP and PVC, photodegradation time, temperature, sun ligth water, initial pH and the presence of some ions were examined. The structure, morphology of the Fe3O4-Bi2WO6 nanocomposite were characterized by powder X-ray diffraction (XRD), scanning electron microscopy (SEM), field emission transmission electron microscopy (FESEM), X-ray photoelectron spectroscopy (XPS) and Fourier transformation infrared spectra (FT-IR) spectroscopy analysis.

The molecular formula of PVC and PP were illustrated in Picture 1.

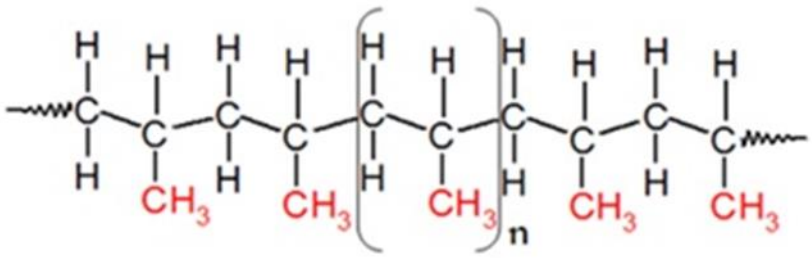

PV

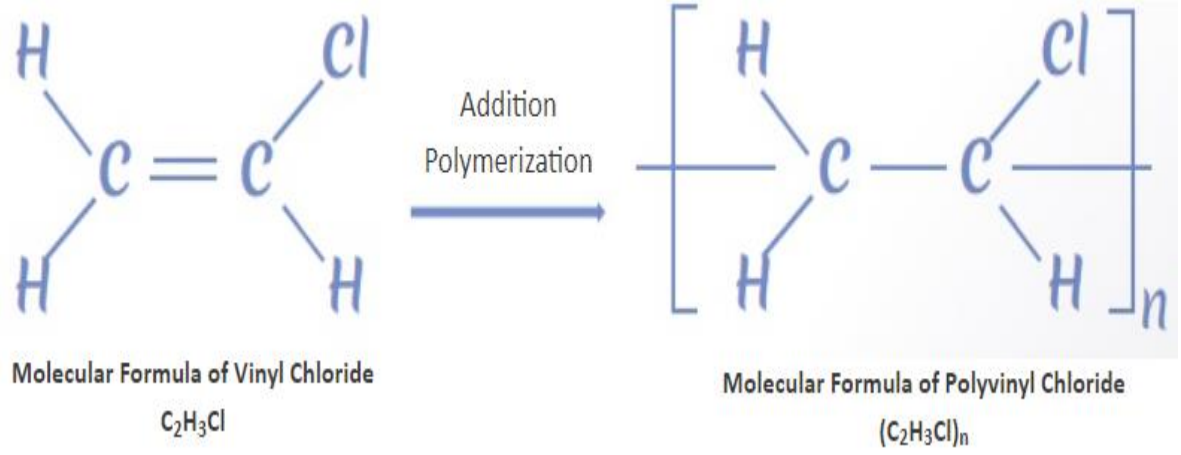

PVC

Materials And Methods

Synthesis of Bi_2WO_6 samples

For Bi_2WO_6 production, 0.98 g $Bi(NO_3)_3 \cdot 5H_2O$ was dissolved in 35 mL distilled water to form a homogeneous solution and stirred for 20 min and sonicated during 40 min. Then 0.33 g $Na_2WO_4 \cdot 2H_2O$ was dissolved in 30 mL and stirred for 40 min. After the pH was adjusted to 6.00. Then, the mixture was maintained at 180 °C for 12 h in an autoclave. The precipitate was rinsed with distilled water and ethanol for four times. The obtained product was dried at 80 °C and denoted as bulk-Bi_2WO_6. Subsequently, the bulk-Bi_2WO_6 samples were calcined at a temperature of 450 °C, for four h. The corresponding products were named as Bi_2WO_6.

Synthesis of Fe_3O_4 Nanosheets

For generation of Fe_3O_4 nanocomposite 69 mmol $Fe(NO_3)_3{\cdot}9H_2O$ was dissolved in 35 mL of the deionized water. It was mixed during 15 min. The pH of the solution was adjusted to 7.0 . Then the mixture was heated in a water bath at 60 °C for 8 h and at 130 °C for 5 h. During heating with N_2 at 600 °C, it was roasted for 6 min. Then Fe_3O_4 nanocomposite was retained.

Synthesis of the Fe_3O_4/Bi_2WO_6 Nanocomposite

In the production of Fe_3O_4/Bi_2WO_6 nanocomposite certain amounts of Fe_3O_4 (0.1, 3, , 9, 12 %) was dissolved in 40 mL of deionized water for 40 min. Then, 0,1 ml of $Bi(NO_3)_3{\cdot}5H_2O$ and $Na_2WO_4{\cdot}2H_2O$ was dissolved into 30 mL 0,1 N HNO_3 and 30 mL of 1 $mol{\cdot}L^{-1}$ NaOH solution, respectively. The $Bi(NO_3)_3{\cdot}5H_2O$ solution and $Na_2WO_4{\cdot}2H_2O$ solution were added to the Fe_3O_4 mixture. After mixing the mixture was cleaned in an autoclave at a temperature of 120 °C for 10 h. The settled chemical was washed with the deionized water. The sample was dried at 50 °C for 14 h. As a result Fe_3O_4/Bi_2WO_6 nanocomposite was obtained.

Characterization of Fe_3O_4/Bi_2WO_6 Nanocomposite

The crystal structure of the nanocomposite was performed by XRD (MerCK, USA) at the angleck, range of 2θ = 8–100° using Cu-Kα irradiation (λ = 0.15418 nm). The morphologies and structures were examined by SEM (Zeiss Sigma HD, Germany) and FESEM (Tecnai G2 F20 S-TWIN TMP, USA). FT-IR was performed on Nicolet iS50 (Thermo Fisher Scientific, USA) spectrophotometer in the range of 400–4000 cm^{-1}. The chemical status and elemental compositions were analyzed by XPS (Thermo Fisher Scientific, USA) with monochromatic Al-Kα source (hv = 1486.6 eV, 6 mA × 12 kV).

Photocatalytic degradation of PVC and PP

The photocatalytic activities of the **Fe_3O_4/Bi_2WO_6 nanocomposite** was investigated by the degradation of PVC and PP under sunligth irradiation. In the experiments certain amount of **Fe_3O_4/Bi_2WO_6 nanocomposite , PVC and PP concentrations** were suspended into 100 mL distilled water. After certain photodegradation times 2 mL of samples were withdrawn and centrifuged.

Measurements of PVC and PP concentrations

For PVC measurements ion chromatography (C-IC) was used.. Hydrogen chloride (HCl) was quantitatively released from PVC during thermal decomposition and trapped in an absorption solution. Selectivity of the marker HCl in complex environmental samples was ensured using cleanup *via* pressurized liquid extraction (PLE) with methanol at 100 °C (discarded) and tetrahydrofuran at 185 °C (collected).The recoveries was around 85.5 ± 11.5% . PP was measured by gas chromatography/ mass spectrometry (Py-GC/MS). Samples was pre-rinsed with analytical grade MilliQ® water (Millipore, Burlington MA, USA) after adding 15 ml of TRIS-HCl buffer (400 mM Tris-HCL, pH 8, 0.5% SDS, Trizbase T6791, HCl H1758, Sigma). The samples were then filtered over a mm GF/F glass fiber filter, diameter 25 mm, mesh size 700 nm (1825–025, Whatman, Maidstone, United Kingdom). To ensure removal of any plastic contamination present, filters were always heated in a 500 °C muffle oven purged with nitrogen prior to filtration.

Results and Discussions

Xrd Results Of Fe_3O_4/Bi_2WO_6 Nanocomposite

XRD analysis were performed to detect the crystallinity of the nanocomposite. The XRD. The diffraction peaks of Bi_2WO_6 at $2\theta = 29.88$, 34.99, 48.77, and 56.11° correspond to the (114), (021), (221), and (315) crystal disturbances of Bi_2WO_6(Figure 1) .The XRD spectra of Fe_3O_4 indicates four peaks at 2θ = 18,88, 31.87, 37.09, and 63.18° corresponding to the (112), (221), (313), and (442) crystal peaks (Figure 1). **The XRD results of Fe_3O_4/Bi_2WO_6 nanocomposite** showed that disturbed Fe_3O_4 was not not visible in the whole nanocomposite indicating the presence of low ratio of the Fe_3O_4. Therefore, the **Fe_3O_4/Bi_2WO_6 nanocomposite** exhibited low crystallinity . This confirm that the cristal structure of **Fe_3O_4/Bi_2WO_6 nanocomposite** originated from the Bi_2WO_6 not from Fe_3O_4.

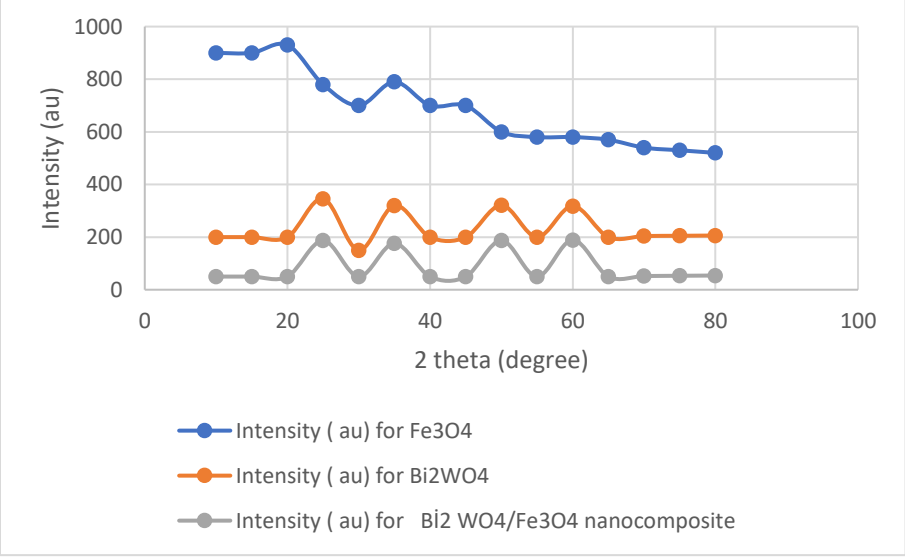

Figure 1: XRD spectra of Fe3O4, Bi2WO4, and Fe3O4/ Bi2WO4 nanocomposite

XPS results of Fe_3O_4/Bi_2WO_6 Nanocomposite

The peaks of XPS spectra of the **Fe_3O_4/Bi_2WO_6 nanocomposite** showed the presence of Fe, W, O, and Bi elements (Figure 2). The peak disturbances relevant to Bi is doped at 162.8 and 166.9 eV, respectively. This showed the presence of Bi^{3+} in the **Fe_3O_4/Bi_2WO_6 Nanocomposite** (Figure 2). The bands at 713.9 and 726.7 eV, can be defined as Fe $2p_{3/2}$ and Fe $2p_{1/2}$. This shows the presence of Fe^{2+} and Fe^{3+}. The existence of Fe^{3+} and Fe^{2+} indicates the presence of Fe_3O_4. The spectrum diagram at 533.9 and 532.6 eV of O 1s indicates the presence of Bi–O

and W–O as $[WO_4]^{2-}$ and $[Bi_2O_2]^{2+}$, respectively. The peak at 527.8 eV is indexed to Fe–O bonds. Fe_3O_4 was witheen Bi_2WO_6 and during phpotooxidation the electrons activated in the holes.

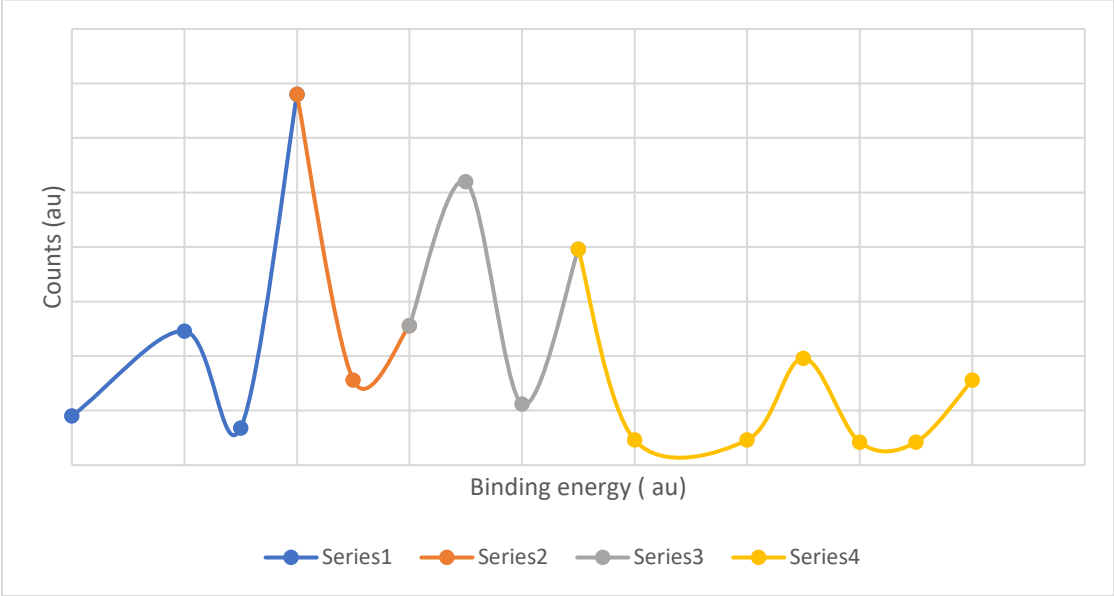

Figure 2: XPS analysis for Seri 1(Counts (au) for W 4f), Seri 2(Counts (au) for Bi W 4f ej, Seri 3(Counts (au) for Bi 4d O 1s) and Seri 4(Counts (au) for Fe 2p

SEM and TEM results of Fe_3O_4/Bi_2WO_6 Nanocomposite

The SEM and TEM images of Fe_3O_4 were illustrated in Figure 3a and 3b,respectively. From Figure 3a a palm shape was observed for **Fe_3O_4/Bi_2WO_6 Nanocomposite. It is uniform structure and every palm** is stacked to the main catalyst. The thickness of the nanocomposite was 35 nm. The negatif charge of the Fe_3O_4 surface leads to the homogen adsorption of Bi^{3+} on the surface of **Fe_3O_4/Bi_2WO_6 Nanocomposite**. In the next steps, Bi^{3+} d react with WO_4^{2-} and Bi_2WO_6 was generated.

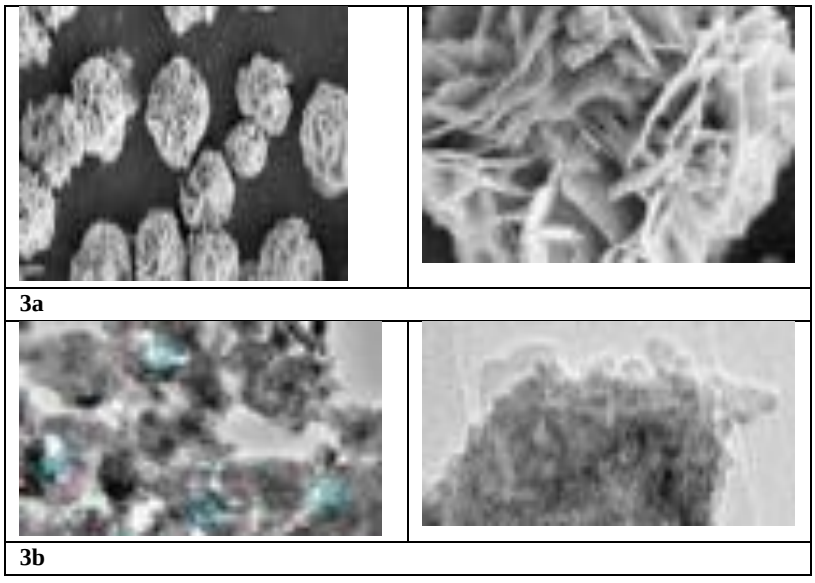

Figure 3: SEM (a) and TEM analyses results of Fe_3O_4/Bi_2WO_6 Nanocomposite

HR-TEM results of Fe_3O_4/Bi_2WO_6 Nanocomposite

HR-TEM analyses (Figure 4a) showed the flake structure of the nanocomposite. The 2D (dimensional)-2D heterostructure of the nanocomposite has a heterojunction structure cause to grow of Bi_2WO_6 around of the Fe_3O_4..The lattice fringes of **Fe_3O_4/Bi_2WO_6 Nanocomposite** corresponded to the (022) plane of Bi_2WO_6. Figure 4b exhibits the Fe, Bi, O and W ingredients. The bonds of the interface between Fe_3O_4 and Bi_2WO_6 facilitate the transfer of electrons and advice the separation of electron–hole pairs during photocatalysis.

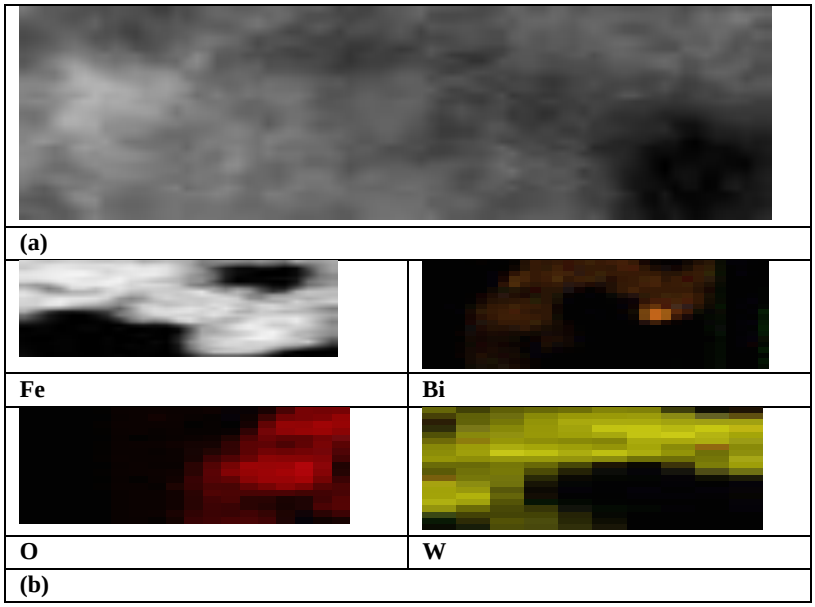

Figure 4: HR-TEM analysis results (a) , Fe, Bi, O and W in the Fe_3O_4 / Bi_2WO_6 nanocomposite Magnetization of Fe_3O_4/Bi_2WO_6 nanocomposite

The magnetization versus magnetic field (M-H loop) for Fe_3O_4/Bi_2WO_6 nanocomposite was shown ın Figure 5. A saturation magnetization (Ms) value of 28 emu/g was obtained, which is higher than Fe_3O_4. The magnetic hysteresis loop indicated a coercivity of 90 Oe. This provides a good separation of Fe_3O_4/Bi_2WO_6 nanocomposite from the liquids with an external magnetic field.

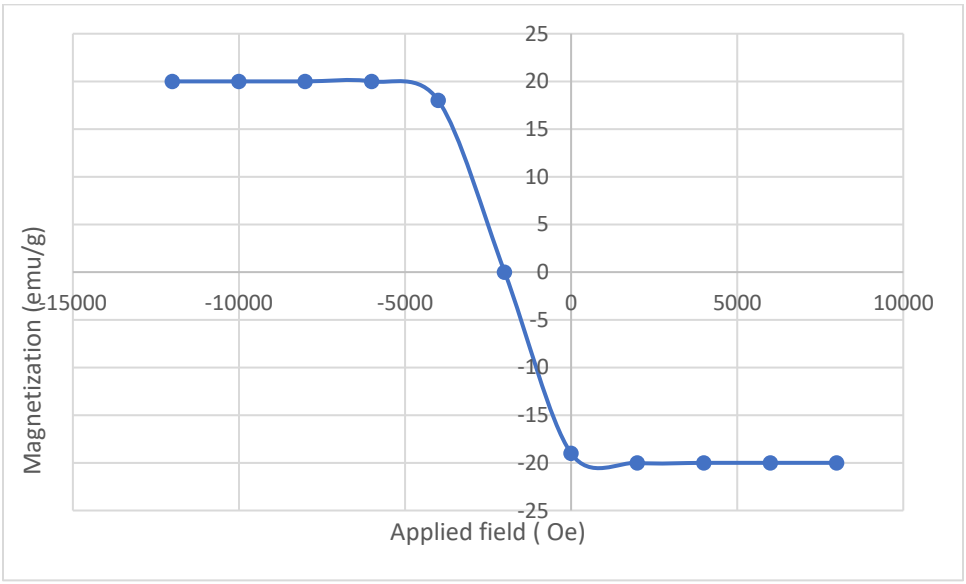

Figure 5: Magnetization versus applied magnetic field for Fe_3O_4/Bi_2WO_6 nanocomposite

FTIR spectra of Fe_3O_4, Bi_2WO_6, and Fe_3O_4/Bi_2WO_6 nanocomposite

The peaks around 573 cm^{-1} can be defined to Fe-O-Fe vibration of magnetite phase. The peak examined near 565 cm^{-1} show the disturbances after photodegradation (Figure 6). The observed shift can be attributed to the binding of PVC and PP to **the surface Fe_3O_4/Bi_2WO_6 nanocomposite. T**he same figure also exhibited the FTIR spectrum relevant to Bi_2WO_6. Observed peaks at 733 cm^{-1} and 578 cm^{-1} are defined by the doping Bi, O and WO, respectively. The peaks at 1380 cm^{-1} and 1628 cm^{-1} were relevant to CH and OH. In Figs. S2c and S2d, the maximum peaks of the **Fe_3O_4/Bi_2WO_6 nanocomposite** detected near 3333 cm^{-1} can be attributed to OH vibration of bonded water. The Bi_2WO_6 bands at 450–1790 cm^{-1} were attributed to BiOBi, WO bondings.After photodegradation the FTIR data of **Fe_3O_4/Bi_2WO_6 nanocomposite indicates the presence of** small amount of organics doped on the surface of nanocomposite.

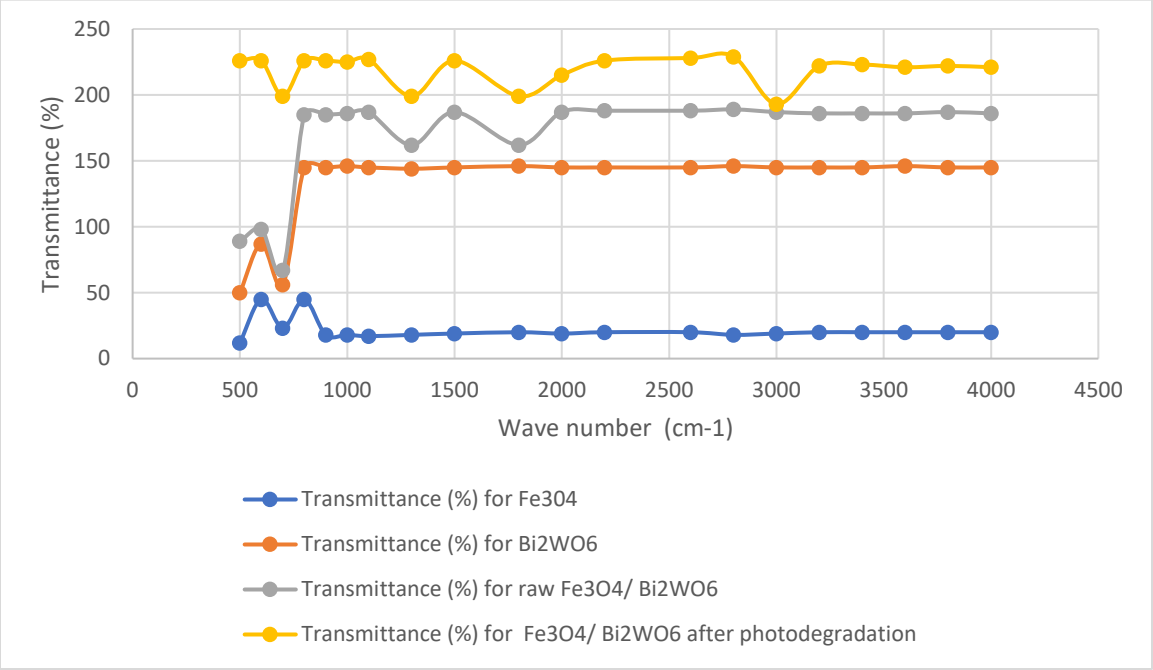

Figure 6: FTIR spectra of Fe_3O_4, Bi_2WO_6, raw Fe_3O_4/Bi_2WO_6 nanocomposite and after photodegradation process Operational conditions affecting the photodegradation of polyvinyl chloride (PVC) and polypropylene (PP)

Effect of pH on the photocatalysis of PVC and PP

The surface of the is positively charged in acidic conditions and negatively charged in the basic medium. Fe_3O_4/Bi_2WO_6 has higher oxidizing activity in lower acidic pH. The optimum pH for maximum photodegradation of **polyvinyl chloride (PVC) and polypropylene (PP) (99% and 98%,respectively)** is 5 whilst exhibited lowest photodegradation at pH 8 (56% and 50%,respectively)(Table 1). At optimal pH, during PVC and PP photodegradation the negatively charged groups of the microplastics strongly interact with the positively charged surface of the Fe_3O_4/Bi_2WO_6 nanocomposite in an acidic medium The pH of zero-point charge (pH_{pzc}) for Fe_3O_4/Bi_2WO_6 nanocomposite is 6.1. Thus, below pH_{pzc}, Fe_3O_4/Bi_2WO_6 nanocomposite surface acquires a positive charge to attract to the negatively charged PVC and PP. Under these conditions PVC and PP concentrated on the Fe_3O_4/Bi_2WO_6 nanocomposite surface. The lectrostatic repulsion between the negatively charged PVC and PP and the negative charge of the Fe_3O_4/Bi_2WO_6 nanocomposite surface above pH_{pzc} retards the doping of the PVC and PP resulting in lower photocatalytic activity. In this study higher pH is not suitable for photodegradation of PVC and PP due to competes with the organic pollutants for getting doped on the Fe_3O_4/Bi_2WO_6 nanocomposite surface. However, lower pH increase the doping PVC and PP, therefore, increase the efficiency of the PVC and PP photodegradations.

pH	**polyvinyl chloride (PVC) photodegradation yields (%)**	**polypropylene (PP) photodegradation yields (%)**
2	67	65
4	84	82
5	99	98
7	67	64
8	56	53
10	23	20

Table 1: Variations of PVC and PP photodegradation yields versus pH

Effect of Fe_3O_4/Bi_2WO_6 nanocomposite concentrations on PVC and PP photodegradation yields

The efficiency of the PVC and PP photodegradation is relevant with Fe_3O_4/Bi_2WO_6 nanocomposite concentrations. As the Fe_3O_4/Bi_2WO_6 nanocomposite concentration was increased the PVC and PP photodegradations yields increased. As the the Fe_3O_4/Bi_2WO_6 concentration was increased from 0,5 mg/l up to 1 and 1.5 mg/l the PVC and PP phodegradation yields were increased from 67%, 64% to 82% , 80% and to 99%, 98%,respectively(Table 2). Further increase of nanocomposite concentrations to 2.0 , 2.5 and 3.0 mg/l did not affect the PVC and PP photodegradation yields. Nanocomposite surface area elevated with the increase in the amount nanocomposite loading. The meaning of the large surface area is the presence of active sites and the presence of high cencentrations of $OH^{\bullet}$ radicals. However, as the Fe_3O_4/Bi_2WO_6 nanocomposite concentration was increased to 2 and 3 mg/l the linear correlation between nanocomposite and microplastics was not detected. Excess concentration of the catalyst turned the solution turbid and increase light dispersion resulting in the lower light penetration for effective photodegradationof PVC and PP.

Fe_3O_4/Bi_2WO_6 nanocomposite concentration (mg/l)	polyvinyl chloride (PVC) photodegradation yields (%)	polypropylene (PP) photodegradation yields (%)
0,5	67	64
1,0	82	80
1,5	99	98
2,0	99	98
2,5	98	97
3,0	98	97

Table2: Variations of **PVC and PP photodegradation yields versus Fe_3O_4/Bi_2WO_6 nanocomposite concentrations**

Effect of Concentrations of PVC and PP on PVC and PP photodegradation yields

For maximal PVC and PP photodegradation yields the optimal PVC and PP concentrations should be studied. The PVC and PP concentrations were increased from 20 mg/l up to 40, 80, 150, 300, 500, 600, 800, 1000, 1200 and 1500 mg/l. As the PVC and PP concentration were increased the pollutant yields were detected as 99 and 98% up to a PVC and PP concentrations of 1200 mg/l,respectively(Table 3). Furher increse of PVC and PP concentrations the microplastic photodegradation yields sligthly decreased to 89% and 88%, respectively. At 20-150 mg/l PVC and PP concentrations the yields of micropollutants were 76% and 75% .Although the photodegradation is lower at a lower initial PVC and PP concentrations the photodegradation yields elevated to a certain micropollutant concentration and then began to decrease at high micropollutant concentrations. Increasing PVC and PP levels cause to doping of these organics on the surface of the nanocomposite . Then ligth penetration coming to nanocomposite surface decreased. The relathionship between PVC and PP and molecules and the active sites of the Fe_3O_4/Bi_2WO_6 nanocomposite is extremely high at low micropollutant concentrations. The the photons and OH radical concentrations going to the Fe_3O_4/Bi_2WO_6 nanocomposite surface also elevated when the micropollutants concentrations were elevated. As a result, these conditions cause to decrease of the photon and OH concentrations reaching on the surface of Fe_3O_4/Bi_2WO_6 nanocomposite ending with low photodegradation yields.

PVC and PP concentrations (mg/l)	polyvinyl chloride (PVC) photodegradation yields (%)	polypropylene (PP) photodegradation yields (%)
20	75	74
40	76	75
80	76	75
150	99	98
300	99	98
500	99	98
600	99	98
800	99	98
1000	89	88
1200	80	79
1500	80	79

Table 3: Effect PVC and PP Concentrations on PVC and PP photodegradation yields

Effect of some ions namely Cl^-, SO_4^{2-}, BrO^{3-}, PO_4^{3-}, CO_3^{2-}, HCO^3 on PVC and PP photodegradation yields

In industries produced microplastics like PVC and PP some chemicals like KCl, Na2SO_4, Bi3BrO, Na3PO_4^{3-}, Ca2CO_3 and NaHO3 were used during polymerisation of raw feding material. However, inorganic ions like Fe^{2+}, Ag^+, Zn^{2+}, Na^+, Cl^-, SO_4^{2-}, BrO^{3-}, PO_4^{3-}, CO_3^{2-}, HCO^{3-} and persulphate ions; some times effect negatively the process or can stimulate the photodegradation efficiency and can be decrease the photodegradation duration. İt was found that low concentrations of Cl^-, SO_4^{2-}, BrO^{3-}, PO_4^{3-}, CO_3^{2-}, HCO^3 ions did not affect (0.1, 0.3, 0.5 , 0.9 mg/l) the photodegradation yields of PVC and PP(Table 4). High concentration of these ions (2, 4 and 6 mg/l) decrease the PVC and PP photodegradation yields to 87% and 85%,respectively. The reason of this can be attributed to the quenching effects for OH radicals. CO_3^{2-}, HCO_3^- lowered the microplastic yields by scavenging the $OH^{\bullet}$ radical productions .

Cl^-, SO_4^{2-}, BrO^{3-}, PO_4^{3-}, CO_3^{2-}, HCO^3concentrations (mg/l)	polyvinyl chloride (PVC) photodegradation yields (%)	polypropylene (PP) photodegradation yields (%)
0,1	99	98
0,3	99	98
0,5	99	98
0,9	99	98
2	87	85
4	87	85
6	84	83

Table 4: Effects of **Cl^-, SO_4^{2-}, BrO^{3-}, PO_4^{3-}, CO_3^{2-}, HCO^3concentrations on PVC and PP photodegradation yields**

Effect of Temperatures on PVC and PP photodegradation yields

In this study, it was found that as the temperature was increased from 15 oC to 22 and to 30oC the phtodegradation yields of PVC and PP increased from 56%, 59% to 99% and from 55% and to 57% and 98% (Table 5). Furher increase of temperature to 40 and 50 oC affected negatively the microplastic photodegradation yields. 80-76% and 79%- 75% photodegradation yields were detected for PP and PVC under aforementioned temperatures. Although increasing of temperature elevated the photodegradation efficiency, higher temperature did not provides to generation of enough OH radicals and continous electron–hole recombinations were not occurred. In heterogeneous photocatalytic systems, temperature was found to have an indirect effect on the photodegradation of microplastics. In particular, low temperatures accelerates the doping of PVS and PP on the surface of Fe_3O_4/Bi_2WO_6 nanocomposite. At elavated the increasing of the disturbing of the PVC and PP microplastics elevates the kinetic energy. The high kinetic energy in the microplastics can be emitted from photodegradation yields.

Temperature (oC)	polyvinyl chloride (PVC) photodegradation yields (%)	polypropylene (PP) photodegradation yields (%)
15	56	55
22	59	57
30	99	98
40	80	79
50	76	75

Table 5: Effect of Temperatures on PVC and PP photodegradation yields

Effect of Sun Light Intensity on PVC and PP photodegradation yields

In this study as the sun ligth intensity increased from10 W/m2 to 20 W/m2 the PVC and PP yields increased from 76% and 74% to 89 and 88% At 40 W/ms sun ligth intensity maximum PVC and PP photodegradation yields was detected as 99% and 98%,respectively(Table 6).. Furher increase of sun ligth intensity to 60 and 80 W/m2 the pollutant yields decreased to 78% and 75%. At 100 W/m2 the yşields decreased to 56% and %54% for PVC and PP, respectively. At high light intensity photons per unit time and unit area decreased ending with low photocatalytic activity.The unwanted electron–hole recombination is high when irradiated at high sun ligth intensity ending with decreased photodegradation yields. At elevated light intensity electron–hole pairs recombination is high thus results with low PVC and PP yields

Sun ligth intensity (W/m2)	polyvinyl chloride (PVC) photodegradation yields (%)	polypropylene (PP) photodegradation yields (%)
10	76	74
20	89	88
40	99	98
60	82	80
80	78	75
100	56	54

Table 6: Variations of PVC and PP photodegradation yields versus Sun Light Intensity

Effect of Irradiation Time on PVC and PP photodegradation yields

The photodegradation capacity of the Fe_3O_4/Bi_2WO_6 nanocomposite versus PVC and PP yields were investigated during irradiation time. The PVC and PP photodegradation yields increased from 59%, 56% to 79%, 76% with an increase in the photodegradation time from 5 min to 10 min (Table 7). After 15 min photodegradation time the yields of PVC and PP reached 99% and 98%,respectively. This attributes to an increase in the formation of more $OH^{\bullet}$ and $O_2^{\bullet-}$ with irradiation time. However, the photodegradatıın yield decreased after an optimum time. This optimum time depends on the catalysts as well as the types of microplastics. After 20 min photodegradation the PVC and PP photodegradation yields decreased sligtly to 90% amd 89%. The reduced rate of degradation after a certain time limit is attributed to the difficulty in the photooxidation of the intermediate products. The photodegrataion efficiency is a function of irradiation time. At the beginning of the photodegradation, high rate formation of $OH^{\bullet}$ process improve the PVC and PP yields. After 20 min OH molecules between surface and bulk phase hindered the filling of remaining active sites in the Fe_3O_4/Bi_2WO_6 nanocomposite.After 30 and 40 min the photodegradation yields tends to a constant value of 79% and 76% for PVC and PP.

Photodegradation time (min)	polyvinyl chloride (PVC) photodegradation yields (%)	polypropylene (PP) photodegradation yields (%)
5	59	56
10	79	76
15	99	98
20	90	89
40	85	83

Table 7: Variation of PVC and PP photodegradation yields versus photodegradation time

Conclusions

The results of PVC and PP photodegradation high photocatalytic activity of Fe3O4/Bi2WO6 nanocomposites under sunlight conditions. The high performance and durability of this composite can be attributed to the high photocatalytic capacity due to enhanced visible sun light absorption. The PVC and PP photodegradation behavior, the influencing factors were investigated in this study.

References

1. Liu Z, Chen F, Gao Y, Liu Y, Fang P. Et al. (2013). A novel synthetic route for magnetically retrievable Bi_2WO_6 hierarchical microspheres with enhanced visible photocatalytic performance. *Journal of Materials Chemistry*. A, Materials for Energy and Sustainability, 1(24): 7027–7030
2. Raizada P, Kumari J, Shandilya P, Dhiman R, Pratap Singh V. et al. (2017). Magnetically retrievable Bi_2WO_6/Fe_3O_4 immobilized on graphene sand composite for investigation of photocatalytic mineralization of oxytetracycline and ampicillin. *Process Safety and Environmental Protection*, 106(Supplement C): 104–116
3. Meng X, Zhang Z. (2017). Synthesis and characterization of plasmonic and magnetically separable $Ag/AgCl-Bi_2WO_6@Fe_3O_{t4}@SiO_2$ coreshell composites for visible light-induced water detoxification. *Journal of Colloid and Interface Science*, 485(Supplement C): 296–307
4. Lu D, Yang M, Kumar K K, Wang H, Zhao X. et al. (2018). aGrape-like Bi_2WO_6/CeO_2 hierarchical microspheres: A superior visible-light-driven photoelectric efficiency with magnetic recycled characteristic. *Separation and Purification Technology*, 194: 130–134
5. Kakroudi MA, Kazemi F, Kaboudin B. (2014). *β*-Cyclodextrin-TiO_2: Green nest for reduction of nitroaromatic compounds. RSC Advances, 4(95): 52762–52769
6. Wang M, Fang G, Liu P, Zhou D, Ma C. et al. (2016). Fe_3O_4@*β*-CD nanocomposite as heterogeneous Fenton-like catalyst for enhanced degradation of 4-chlorophenol (4-CP). Applied Catalysis B: *Environmental*, 188: 113–122
7. Kong L, Fang G, Kong Y, Xie M, Natarajan V. et al. (2018). Cu_2O@*β*-cyclodextrin as a synergistic catalyst for hydroxyl radical generation and molecular recognitive destruction of aromatic pollutants at neutral pH. *Journal of Hazardous Materials*, 357: 109–118
8. Yu C, Bai Y, Chen J, Zhou W, He H. et al. (2015). Pt/Bi_2WO_6 composite microflowers: High visible light photocatalytic performance and easy recycle. Separation and Purification Technology, 154: 115–122
9. Tada H. (1960). Decomposition reaction of hexamine by acid. Journal of the American Chemical Society, 82(2): 255–263
10. Mahfouz R M, Al-Hokbany N S, Siddiqui M R H. (2011). Corals of In_2O_3 nanoparticles, synthesis by the thermal decomposition of *γ*-irradiated indium acetate in the presence of a nonaqueous medium. Synthesis and Reactivity in Inorganic, Metal-Organic, and Nano-Metal Chemistry, 41(7): 858–863
11. Galvão J G, Silva V F, Ferreira S G, França F R M, Santos D A. et al. (2015). *β*-Cyclodextrin inclusion complexes containing *Citrus sinensis* (L.) osbeck essential oil: An alternative to control *Aedes aegypti* larvae. Thermochimica Acta, 608: 14–19
12. Liu L, Ding L, Liu Y, An W, Lin S. et al. (2016). Enhanced visible light photocatalytic activity by Cu_2O-coupled flower-like Bi_2WO_6 structures. Applied Surface Science, 364: 505–515
13. Sun Q, Jia X, Wang X, Yu H, Yu J. (2015). Facile synthesis of porous Bi_2WO_6 nanosheets with high photocatalytic performance. Dalton Transactions (Cambridge, England), 44(32): 14532–14539
14. Li Y, Liu J, Huang X, Li G. (2007). Hydrothermal synthesis of Bi_2WO_6 uniform hierarchical microspheres. Crystal Growth & Design, 7(7): 1350–1355
15. Tang J, Zou Z, Ye J. (2004). Photocatalytic decomposition of organic contaminants by Bi_2WO_6 under visible light irradiation. Catalysis Letters, 92(1): 53–56
16. Zhang L, Wang W, Zhou L, Xu H. (2007). Bi_2WO_6 nano- and microstructures: Shape control and associated visible-light-driven photocatalytic activities. Small, 3(9): 1618–1625
17. Zhang C, Zhu Y. (2005). Synthesis of square Bi_2WO_6 nanoplates as highactivity visible-light-driven photocatalysts. Chemistry of Materials, 17(13): 3537–3545
18. Chen C, Cao S, Yu W, Xie X, Liu Q. et al. (2015). Adsorption, photocatalytic and sunlight-driven antibacterial activity of Bi_2WO_6/graphene oxide nanoflakes. Vacuum, 2015, 116: 48–53
19. Zhang L, Wang H, Chen Z, Wong P K, Liu J. (2011). Bi_2WO_6 micro/nanostructures: Synthesis, modifications and visible-light-driven photocatalytic applications. Applied Catalysis B: Environmental, 106(1-2): 1–13
20. Xu X, Shen X, Zhu G, Jing L, Liu X. et al. (2012). Magnetically recoverable Bi_2WO_6-Fe_3O_4 composite photocatalysts: Fabrication and photocatalytic activity. *Chemical Engineering Journal*, 200-202: 521–531
21. Dong P, Hou G, Xi X, Shao R, Dong F. (2017). WO_3-based photocatalysts: Morphology control, activity enhancement and multifunctional applications. *Environmental Science. Nano*, 4(3): 539–557
22. Song G, Wu X, Xin F, Yin X. (2017). $ZnFe_2O_4$ deposited on BiOCl with exposed (001) and (010) facets for photocatalytic reduction of CO_2 in cyclohexanol. *Frontiers of Chemical Science and Engineering*, 11(2): 197–204
23. Liu Y, Wei B, Xu L, Gao H, Zhang M. (2015). Generation of oxygen vacancy and OH radicals: A comparative study of Bi_2WO_6 and Bi_2WO_{6-x} nanoplates. *ChemCatChem*, 7(24): 4076–4084
24. Zhang Y, Zhang N, Tang Z R, Xu Y J. (2013). Identification of Bi_2WO_6 as a highly selective visible-light photocatalyst toward oxidation of glycerol to dihydroxyacetone in water. *Chemical Science (Cambridge)*, 4(4): 1820–1824
25. Kumar A, Guo C, Sharma G, Pathania D, Naushad M. et al. (2016). Magnetically recoverable ZrO_2/Fe_3O_4/chitosan nanomaterials for enhanced sunlight driven photoreduction of carcinogenic Cr(vi) and dechlorination & mineralization of 4-chlorophenol from simulated waste water. RSC Advances, 6(16): 13251–13263
26. Wu W, Changzhong J, Roy V A. (2015). Recent progress in magnetic iron oxide-semiconductor composite nanomaterials as promising photocatalysts. Nanoscale, 7(1): 38–58
27. Chalasani R, Vasudevan S. (2013). Cyclodextrin-functionalized Fe_3O_4@-TiO_2: Reusable, magnetic nanoparticles for photocatalytic degradation of endocrine-

disrupting chemicals in water supplies. ACS Nano, 7(5): 4093–4104

28. Meng X, Qin H, Zhang Z. (2018). New insight into the enhanced visible light-driven photocatalytic activity of Pd/$PdCl_2$-doped Bi_2WO_6 photocatalysts. *Journal of Colloid and Interface Science*, 513: 877–890
29. Meng X, Li Z, Zeng H, Chen J, Zhang Z. (2017). MoS_2 quantum dotsinterspersed Bi_2WO_6 heterostructures for visible light-induced detoxification and disinfection. *Applied Catalysis B: Environmental*, 210: 160–172
30. Zhou Y X, Tong L, Zeng X H, Chen X B. (2015). Fe_3O_4@Bi_2WO_6 coreshell structured microspheres: Facile construction and magnetically recyclable photocatalytic activity under visible-light. *Journal of Nanoscience and Nanotechnology*, 15(12): 9868–9873
31. Chen S H, Yin Z, Luo S L, Au C T, Li X J. (2013). Preparation of magnetic Fe_3O_4/SiO_2/Bi_2WO_6 microspheres and their application in photocatalysis. *Materials Research Bulletin*, 48(2): 725–729
32. Zhang L, Wang W, Shang M, Sun S, Xu J. (2009). Bi_2WO_6@carbon/Fe_3O_4 microspheres: Preparation, growth mechanism and application in water treatment. *Journal of Hazardous Materials*, 172(2): 1193–1197
33. Liu Z, Chen F, Gao Y, Liu Y, Fang P. et al. (2013). A novel synthetic route for magnetically retrievable Bi2WO6 hierarchical microspheres with enhanced visible photocatalytic performance. Journal of Materials Chemistry. A, *Materials for Energy and Sustainability*, 1(24): 7027–7030
34. Raizada P, Kumari J, Shandilya P, Dhiman R, Pratap Singh V. et al. (2017). Magnetically retrievable Bi2WO6/Fe3O4 immobilized on graphene sand composite for investigation of photocatalytic mineralization of oxytetracycline and ampicillin. Process Safety and Environmental Protection, 106(Supplement C): 104–116
35. Meng X, Zhang Z. (2017). Synthesis and characterization of plasmonic and magnetically separable Ag/AgCl-Bi2WO6@ Fe3O4@SiO2 coreshell composites for visible light-induced water detoxification. *Journal of Colloid and Interface Science*, 485(Supplement C):
36. Lu D, Yang M, Kumar K K, Wang H, Zhao X. et al. (2018). Grapelike Bi2WO6/CeO2 hierarchical microspheres: A superior visiblelight-driven photoelectric efficiency with magnetic recycled characteristic. Separation and Purification Technology, 194: 130–134
37. Liu Y, Wei B, Xu L, Gao H, Zhang M. (2015). Generation of oxygen vacancy and OH radicals: A comparative study of Bi2WO6 and Bi2WO6 – x nanoplates. *ChemCatChem*, 7(24): 4076–4084 49.
38. Zhang Y, Zhang N, Tang Z R, Xu Y J. (2013). Identification of Bi2WO6 as a highly selective visible-light photocatalyst toward oxidation of glycerol to dihydroxyacetone in water. *Chemical Science (Cambridge)*, 2013, 4(4): 1820–1824
39. Kumar A, Guo C, Sharma G, Pathania D, Naushad M. et al. (2016). Magnetically recoverable ZrO2/Fe3O4/chitosan nanomaterials for enhanced sunlight driven photoreduction of carcinogenic Cr(vi) and dechlorination & mineralization of 4-chlorophenol from simulated waste water. RSC Advances, 6(16): 13251–13263 51.
40. Wu W, Changzhong J, Roy V A. (2015). Recent progress in magnetic iron oxide-semiconductor composite nanomaterials as promising photocatalysts. Nanoscale, 7(1): 38–58